Scientific report; WR 97-03

KNMI

SATVIEW:
a semi-physical scatterometer algorithm

J.A.M. Janssen and
H. Wallbrink

De Bilt, 1997

Scientific report = wetenschappelijk rapport; WR 97 - 03

De Bilt, 1997

P.O. Box 201
3730 AE De Bilt
Wilhelminalaan 10
Telefoon 030-220 69 11
telefax 030-221 04 07

Authors: J.A.M. Janssen and
H. Wallbrink

UDC: 551.507.362.2
551.46.062.5
551.501.75
551.466.33

ISSN: 0169-1651

ISBN: 90-369-2121 -X

SATVIEW, a semi-physical scatterometer algorithm

J.A.M. Janssen
and
H. Wallbrink

Royal Netherlands Meteorological Institute
De Bilt
The Netherlands

February 1997

Abstract

A long term objective of scatterometry is to uncover its underlying physics. The route to achieve this is dotted with numerous pitfalls, as has been established by several extensive studies. Also KNMI prominently supported one of those studies by developing a proto-type scatterometer algorithm. The merits and demerits of this VIERS model will be recapitulated.

The SATVIEW study was intended to eliminate, or and least mitigate, the remaining problem from which the successive cycles of the VIERS algorithm still suffered. The present report gives an account of the possible solutions and the benefits obtained.

The SATVIEW modifications improve the working of the scatterometer algorithm, but are based on parametrizations of certain key-processes. One such key-process is angular wave spreading; by a careful study of ERS-1 data its complex structure has been revealed.

Although thus an important step has been made towards a better understanding of the role of water waves in the backscatter process, from a fundamental point of view the physics of the scatterometer still contains unresolved issues. The present algorithm should therefore be classified as a semi-physical one. Further steps require more research in air-sea interaction processes.

Contents

List of Figures

List of Tables

1 Introduction

The SATVIEW project is a continuation of the extended VIERS project, which has been described in a number of progress reports (Van Halsema et al., 1989, Calkoen et al., 1990, Snoeij et al., 1992, P. Janssen et al., 1994, P. Janssen et al., 1995). In the VIERS project, a joint enterprise of a number of institutes, radar backscattering from a water surface has been investigated both experimentally and theoretically.

Three major experiments have been performed in which the scale of the test-site was successively increased. Primary experiments were conducted in a laboratory flume (Van Halsema et al., 1989). Subsequently the effect of real-sized ocean waves has been simulated and investigated in a large outdoor facility (Calkoen et al., 1990). Finally the step towards field conditions has been made (Snoeij at al., 1992).

The experimental work has been supported by theoretical studies. In the laboratory it has been found that a, more or less standard, two-scale model for radar backscatter based on the Bragg mechanism performed relatively best (J. Janssen et al., 1993). For the wind-wave interaction a bipartite wave model has been developed in which the gravity and capillary part of the wave spectrum are separately calculated and subsequently joined continuously (P. Janssen et al., 1995).

On the basis of these experimental and theoretical studies the VIERS group manufactured an ERS-dedicated scatterometer algorithm. The proto-type has been assembled and configured such that it produces unsuspicious winds, i.e. comparable to CMOD4 retrieved winds.

However, the final VIERS algorithm, cycle 2.0, still suffers from a serious drawback: the cone-shaped manifolds in $\vec{\sigma}$-space (Cavanie et al., 1987) are insufficiently reproduced. It has been recognized that this misfit originates from a defective directional distribution of the short resonant water waves: the VIERS distribution, being wavelength independent, appears to have a too simple structure (P. Janssen et al., 1995).

The motivation for the SATVIEW project is to improve the working of the VIERS algorithm by modifying the directional distribution of the short water waves. This goal was already recommended in the final VIERS-1 report (P. Janssen et al., 1995).

The VIERS and SATVIEW studies fit into a broader context. After the usefulness of the scatterometer as a wind measuring device had been empirically demonstrated, the next step was to explore and understand the physics of scatterometry. An extensive and succesful study was carried out by Donelan and Pierson (D & P, 1987), which showed the feasibility of a two-scale Bragg scattering mechanism combined with a simplified energy balance for the resonant water waves. In fact, the pioneering Donelan and Pierson study was one of the main sources of inspiration for VIERS and SATVIEW, amongst others (cf. Van Halsema et al., 1989).

Another recent project that builds on the framework set out by Donelan and Pierson, was carried out by Barthel and Breivik (B & B, 1996). Their model has two fine points: it takes advantage of inputted wave information from a numerical model and it includes the upwind-downwind contrast by taking into account the tilt-hydrodynamic

modulation of short waves by long waves. The VIERS-SATVIEW algorithm also makes use of wave data (WAM), but the upwind-downwind assymmetry has been neglected.

The present report is intended to describe in considerable, but not full, detail the route towards a scatterometeralgorithm that is able to retrieve wind fields in a reliable and consistent manner. Most part of that route was covered during the VIERS project; SATVIEW was taken up to finish the last part. In order to give the reader an overview of the full route, we will first summarize the theoretical background of the VIERS model and the practical simplifications and approximations that have been made (section 2). In the third section a qualitative account is given of the provisions that had to be made to overcome various tuning problems. Model validation is the subject of the fourth section; it recalls the misfit in VIERS cycle 2.0. The fifth section describes the SATVIEW approach to eliminate it. In the final section we conclude that a lot of practical problems have been solved, but that fundamental issues remain to be answered.

2 Model description

The VIERS model relates radar backscatter to windvector, measurement geometry (=incidence angle), sea state (period of the dominant waves), and other environmental parameters like sea- and air-temperature, humidity, salinity and slicks. In the so-called interpretative mode the windvector $\vec{U}_{10}$, incidence angle θ and wave period P appear at the input level, whereas the normalized cross-section for radar backscatter σ_0 is the output variable. In principle actual information on other environmental parameters (e.g. temperatures T_{sea} and T_{air}, humidity H, salinity S) could also be inputted, but this option has not been effectuated in the first generation VIERS model that will be described here. The reason is that the dependence of radar backscatter on these parameters is not expected to be very dramatic; therefore the values of environmental parameters have been estimated from average climatic conditions.

The relationship between backscatter and the basic input variables is established in three consecutive steps, each with its own submodel. First comes the submodel (wind-stress module) that relates windspeed and wave period to wind stress at the water surface (parameter u_*). In the HEXOS experiment a sea-state dependent roughness length was proposed (Smith et al., 1992); the HEXOS parametrisation has been adopted and implemented into the VIERS model. It should be born in mind that later investigations have cast doubts about the validity of the HEXOS formula (J. Janssen, 1996).

The second submodel is the stress-waves module. Here the full (i.e. both gravity and gravity-capillary waves) spectrum of water waves is determined from wind stress and wave period. The gravity part is obtained by invoking a JONSWAP spectrum, the parameters of which are assumed to depend on wave age. The JONSWAP function is assumed to satisfactory describe the wave spectrum up to the frequency f_{join} ($f_{\text{join}} \approx 2 - 5$ Hz). The grav-cap part is separately obtained by solving an energy-balance equation that includes all relevant processes (i.e. wind input, wave breaking, viscous dissipation, nonlinear wave-wave interactions, dissipation by slicks). The resulting grav-cap part of the spectrum is continously joined to the gravity part at f_{join}. It should be noted that this is only a schematic picture; in practice the calculations are performed in wavenumber space. The transformation to frequency space is, however, straightforward.

Finally the structure of the water surface, descibed by the wave spectrum, has to be related to the radar backscatter (σ_0). This is done in the third submodel, the waves-scatter module. In VIERS a more or less standard two-scale approach had been adopted in which the waves are separated into short and long ones. The short waves that obey the Bragg criterion resonantly scatter the radar beam, whereas the long waves act as facets that tilt the short ones.

The structure of the VIERS interpretative model is summarized in figure 1.

For practical purposes (wind retrieval from ERS-1 scatterometer measurements) the interpretative model has to be inverted (i.e. in- and output have to be interchanged). In order to produce an optimal windvector the inverted VIERS model asks for three

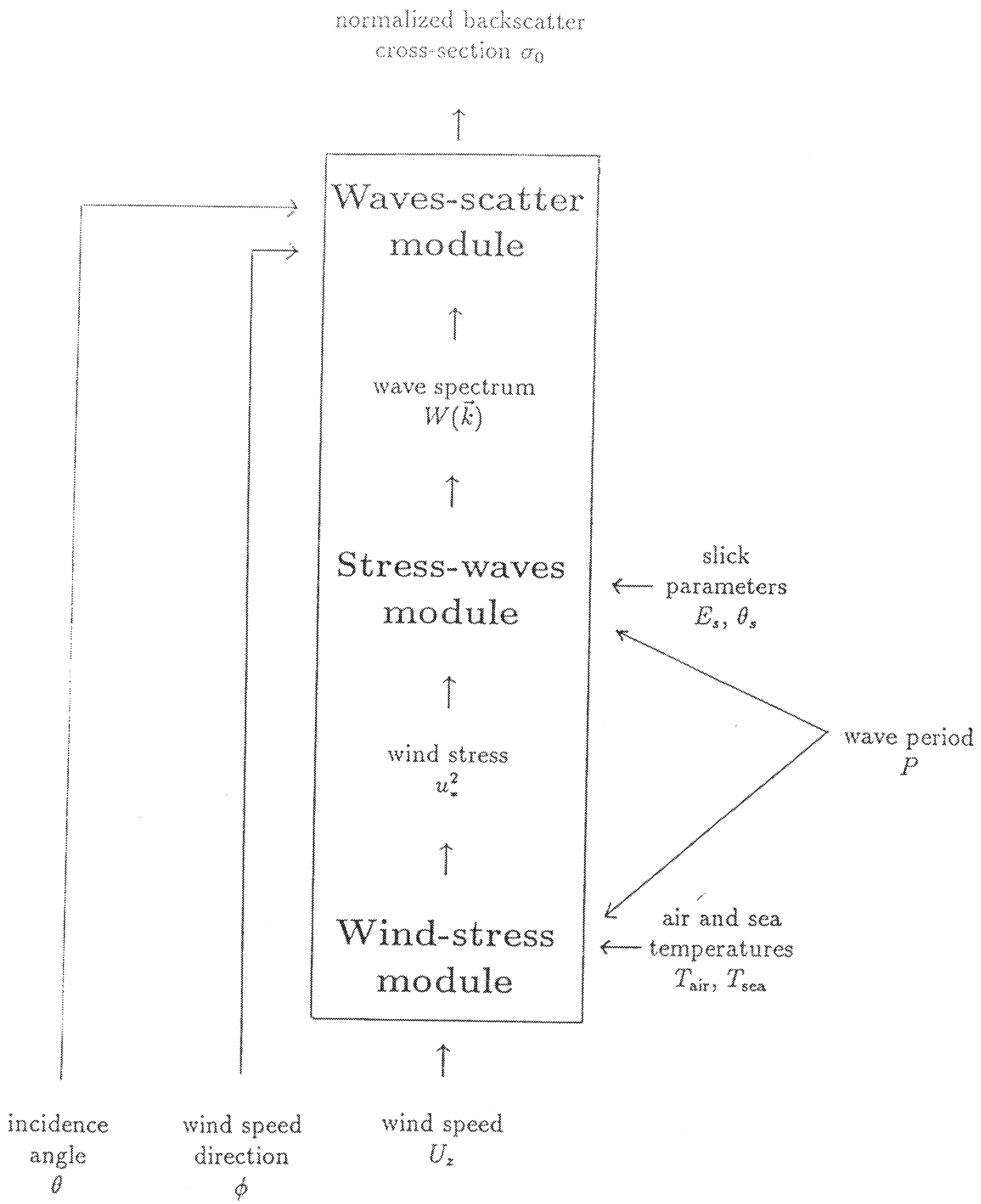

Figure 1: Structure of VIERS interpretative model.

σ_0's (normalized cross-section of respectively for-, mid- and aftbeam) plus the period of the dominant waves. The inversion procedure is a very simple and straightforward one and will be described in detail later on.

2.1 Wind-stress module

The stress field at the air-sea interface is assumed to depend on the wind speed, the stability of the air colomn (air-sea temperature difference) and the sea state (wave age of the dominant waves). For given wind velocity U_z measured at height z, period of the dominant waves P and the temperatures of sea and air (T_{sea} and T_{air}) the VIERS module yields the friction velocity u_*, the roughness length z_0 and the Monin-Obukov stability length L.

The wind profile is assumed to have the following form:

$$U_z = \frac{u_*}{\kappa}(\log(z/z_0) - \Psi_M(z/L)) \tag{1}$$

For the roughness length the HEXOS parametrisation has been adopted (Smith et al., 1992).

$$z_0 = 0.48\frac{2\pi u_*^3}{g^2 P} \tag{2}$$

For the stability parameter Ψ_M the Businger-Dyer expression (Businger et al., 1971; Dyer et al., 1970) has been adopted.

$$\begin{aligned} \Psi_M &= -4.7z/L && \text{(stable)} \\ \Psi_M &= 2\log((1+\Phi_M)/2) + \log((1+\Phi_M^2)/2) - 2\text{atan}(\Phi_M) + \pi/2 && \text{(unstable)} \\ \text{with} \quad \Phi_M &= (1-16z/L)^{0.25} && (3) \end{aligned}$$

The Monin-Obukov length is computed according to Stewart (1985).

$$L = \frac{-U_z u_*}{g\kappa}\frac{T_{air}}{T_{sea} - T_{air}} \tag{4}$$

The equation for the wind profile is solved iteratively in order to obtain a self consistent value for the friction velocity.

2.2 Stress-waves module

The full wave spectrum is determined from the wind stress and the mean period of the dominant waves (P_{mean}). As is well-known from spectra of water waves the mean period is not equal to the peak period of the dominant waves. In VIERS the peak period P is assumed to be 20% larger: $P = 1.2P_{\text{mean}}$.

From peak period P and friction velocity u_*, the wave age ξ is obtained as

$$\xi = \frac{gP}{2\pi u_*} \tag{5}$$

It is assumed that the 1-D gravity part may be well parametrized by a JONSWAP function (Hasselmann et al., 1973).

$$E_{\mathrm{JON}}(f) = \frac{\alpha g^2}{(2\pi)^4 f^5} \exp[-\frac{5}{4}(\frac{f_p}{f})^4]\gamma^r \tag{6}$$

where

$$r = \exp[-\frac{(f-f_p)^2}{2\sigma^2 f_p^2}]$$

The JONSWAP form contains two factors: the Pierson-Moskowitz expression (Pierson and Moskowitz, 1964) and the so-called "peak enhancement factor" γ^r. For old waves γ approaches 1, but for young waves there is a considerable enhancement of the peak ($\gamma \approx 3$).

Contrary to the JONSWAP experiment, in which the peak frequency f_p (or friction velocity u_*) and dimensionless fetch were used as independent parameters, in VIERS the shape parameters f_p, α, γ, σ depend on the alternative independent parameters P and ξ.

$$f_p = P^{-1} \tag{7}$$

$$\alpha = A\xi^{-B} \tag{8}$$

$$\gamma = \max(1, 1 + 3(1 - (0.038\xi)^2)) \tag{9}$$

$$\sigma = 0.08 \tag{10}$$

Remark 1: in the final VIERS-1 report (P. Janssen et al., 1995) a typing error with respect to the ξ-dependence of γ has sneaked in; (9) gives the correct formula.

Remark 2: the parametrisation for the Phillips constant α has not been adopted from the JONSWAP experiment; A and B have been used as tuning parameters with the proviso $0.5 < B < 1.5$.

Although the validity of the JONSWAP function is only forseen up to frequencies of the order of three times the peak frequency, in VIERS the assumption has been made that Phillips' dimensional arguments for the spectral saturation of gravity waves (Phillips, 1958) apply up to the beginning of the grav-cap range (i.e. 2 to 5 Hz). Note that this can be as high as $20 f_p$.

Beyond the frequency f_{join} ($2 < f_{\mathrm{join}} < 5$) a new regime is entered. In this regime it is assumed that the spectral energy is determined by an energy balance that is both stationary and homogeneous and includes the 3-wave interactions. Theoretical details have been given in the third VIERS progress report (Snoeij et al., 1992). Here only a brief resumé will be given.

In the regime of grav-cap waves the energy balance takes the following form.

$$0 = \frac{\partial F}{\partial t} + \vec{v}_g \cdot \frac{\partial F}{\partial \vec{x}} = S_{in} + S_{nl} + S_{dis} \tag{11}$$

F is the 1-D wavenumber spectrum, normalized as $\int_0^\infty kF\,\mathrm{d}k = E_v$ (E_v=variance wave field), and v_g is the group velocity. The source term has been split into a wind input (S_{in}), a nonlinear interactions (S_{nl}) and a dissipation term (S_{dis}).

For S_{in} Plant's expression (Plant, 1980) has been adopted.

$$S_{in} = \beta F \qquad \beta = \delta\omega\frac{u_*^2}{c^2} \tag{12}$$

In which ω is the circular frequency and c the phase speed of the generated wave. The dimensionless constant δ is 0.03. The quasi-linear effect can be incorporated by renormalizing δ (cf. P. Janssen et al., 1989).

It is assumed that S_{nl} may be well represented by a local (in k-space) expression.

$$S_{nl} = -\frac{1}{k}\frac{\partial}{\partial k}\varepsilon(k) \tag{13}$$

Where $\varepsilon(k)$ is the energy flux (in k-space). Assuming that only three- and four-wave interactions contribute one arrives at the following expression for ε.

$$\varepsilon(k) = \frac{c^4}{v_g}(\alpha_3(k^4F)^2 + \alpha_4(k^4F)^3) \tag{14}$$

α_3 and α_4 are dimensionless "coupling constants".

There are three dissipative processes that play a role in the grav-cap regime: viscous damping, wave breaking and damping due to slicks.

$$S_{dis} = S_{vis} + S_{br} + S_{sl} \tag{15}$$

For viscous damping one has the following exact expression (Lamb, 1932).

$$S_{vis} = -4\nu k^2 F \tag{16}$$

ν is the kinematic viscosity of water.

Slick damping is determined by the Marangoni effect (Alpers and Hühnerfuss, 1989). A visco-elastic Marangoni wave extracts energy from the water waves, which therefore effectively experience an additional viscous damping.

$$S_{sl} + S_{vis} = -4\nu_{\text{eff}}k^2F = -4\nu y(f)k^2F \tag{17}$$

$y(f)$ is the relative damping ratio, given by

$$y(f) = \frac{1 + X(\cos\delta - \sin\delta) + XY + Y\sin\delta}{1 + 2X(\cos\delta - \sin\delta) + 2X^2} \tag{18}$$

δ is the phase angle and

$$X = |\frac{E_s}{\rho_w}| \frac{k^2}{\sqrt{2\nu\omega^3}} \tag{19}$$

$$Y = |\frac{E_s}{\rho_w}| \frac{k}{4\omega\nu} \tag{20}$$

E_s is the dilatational modulus of the surface film and ρ_w the density of the water.

Hence a surface film is determined by the two parameters δ and E_s. The phase angle δ is approximately 180^o whereas E_s depends strongly on the biochemical constitution of the slick. For a natural slick (mostly of biological origin) E_s can be estimated to have a value < 0.01 N/m, whereas for chemical slicks the value can vary from 0.01 to 0.05 N/m. Hence the maximal value for $y(f)$ varies from 20 ($E_s = 0.01$) to 40 ($E_s = 0.05$).

Wave breaking is hard to model on physical grounds. For gravity waves Komen et al. (1984) suggest the following expression with $n = 2$.

$$S_{\text{dis}} = -a\bar{\omega}(\frac{\omega}{\bar{\omega}})^n(\frac{\hat{\alpha}}{\alpha_{\text{PM}}})^n F(k) \tag{21}$$

Where a and α_{PM} are constants and

$$\hat{\alpha} = \frac{E_v\bar{\omega}^4}{g^2} \tag{22}$$

E_v is the variance and $\bar{\omega}$ is the mean circle frequency of the wave field.

For the VIERS application the above expression (with $n = 2$) has been generalized for gravity-capillary waves. It reads:

$$S_{\text{dis}} = -\beta_1 E_v^2\bar{\omega}^7\frac{k}{g^3} \tag{23}$$

The constant β_1 should be of the order of 2 to produce realistic spectral tails.

As an alternative parametrisation for wave breaking the following expression has also been investigated ("quadratic breaking").

$$S_{\text{dis}} = -\beta_2 E_v^2\bar{\omega}^5\frac{k^2}{g^2} \tag{24}$$

It is, however, impossible to produce realistic spectra with this model because the breaking is too violent at high windspeeds. Hence, $\beta_2 = 0$.

If one uses the explicit expressions for the source terms, the energy balance attains the following form.

$$\frac{\partial}{\partial k}\varepsilon(k) = \gamma c^2 k^2 F \tag{25}$$

The coefficient γ is defined as

$$\gamma = \delta\omega\frac{u_*^2}{c^2} - 4\nu y(f)k^2 - \beta_1\bar{\omega}^7\frac{E_v^2}{g^3}k \tag{26}$$

Hence it gives the net effect of wind input and dissipation. The energy flux $\varepsilon(k)$ is given by

$$\varepsilon(k) = c^2 v_g(\alpha_1 S^2 + \alpha_2 S^3) \qquad S = \frac{c}{v_g}k^4 F \tag{27}$$

The coupling constants for the three- and four-wave interactions have been modelled as

$$\alpha_1 = T_3 \frac{\pi}{16}(\tanh(\Sigma(x-1))+1) \qquad x = \frac{f}{f_x}$$
$$\alpha_2 = T_4 \tag{28}$$

It can be argued that the frequency f_x at which the three-wave interactions are turned on, should be put equal to $f_{3W} = \frac{1}{2\pi}(g\sqrt{g/2T})^{1/2} \approx 7$ Hz (T is surface tension). Several tuning exercises have learned, however, that $f_x = f_{\text{join}} \approx 2-5$ Hz works out better.

The width parameter Σ should be high enough to ensure smooth wave spectra; typical values are in the range 2 (VIERS cycle 2.0) to 4 (SATVIEW).

Special discussion deserve the parameters that measure the strength of the three- and four-wave interactions: T_3 and T_4. In principle they are tuning parameters, but in order to get a balanced influence of non-linear interactions their values should be of order 1. One may give constant values to T_3 and T_4, but their is nothing against building in a wind speed dependence. This latter option has been picked up in SATVIEW.

In order to obtain a unique solution of the above energy balance, its equation has to be supplemented with a boundary condition, viz. the continuity of the spectrum at $k = k_{\text{join}}$. Obviously, this separating point in wavenumber space corresponds to the separating frequency f_{join} in frequency space via the dispersion relation.

The solution of the energy balance equation is the 1-D wavenumber spectrum $F(k)$. If one ignores the frequency shifting (=Doppler) effect due to the orbital motion of the long waves, $F(k)$ may be related to the 1-D frequency spectrum $E(f)$ as follows.

$$\frac{2\pi k}{v_g} F(k) = E(f) \tag{29}$$

Having found the 1-D frequency spectrum in the grav-cap range of frequencies ($f > f_{\text{join}}$), one may combine it with the JONSWAP spectrum in the gravity range ($f < f_{\text{join}}$) to obtain the full spectrum.

In order to statistically describe the structure of the water surface a 1-D wavenumber spectrum is not sufficient: the directional distribution of the waves has to be included. In the VIERS model the simplifying assumption has been made that the 2-D wavenumber spectrum is separabel.

$$W(k,\alpha) = F(k)D(\alpha) \tag{30}$$

Where

$$D(\alpha) = \frac{1}{2\pi}(1 + 2a_2 \cos 2(\alpha - \alpha_W)) \tag{31}$$

α_W is the direction of the wind. The parameter a_2 measures the width of the directional distribution. As a simplification in VIERS it is assumed that a_2 only depend on stress, not on frequency; in SATVIEW this restriction was relaxed.

2.3 Waves-scatter module

Once the 2-D wave spectrum is known the next step is to determine the normalized backscatter from it. This asks for a module that models the scattering process. In VIERS a two-scale model has been chosen. According to the 'wave-facet model' (Valenzuela, 1978; Plant, 1990) the following expression for the normalized cross-section applies.

$$\sigma_0^{\mathrm{SEA}} = \sigma_0^{\mathrm{sp}} + \int_{-\infty}^{\infty} d(\tan\psi) \int_{-\infty}^{\infty} d(\tan\delta) P_B(\tan\psi, \tan\delta) \sigma_0^{\mathrm{Br}}(\theta_{\mathrm{loc}}) \tag{32}$$

Where P_B is the probability that a (Bragg-)facet is oriented with tilts $\tan\psi$ (parallel) and $\tan\delta$ (right angles to the wind). θ_{loc} is the local incidence angle. For an anisotropisch Gaussian surface one has:

$$P_B = \frac{1}{2\pi s_{u,b} s_{c,b}} \exp(-\frac{\tan^2\psi}{2s_{u,b}^2} - \frac{\tan^2\delta}{2s_{c,b}^2}) \tag{33}$$

In which $s_{u,b}^2$ and $s_{c,b}^2$ are the slope variances in the upwind and crosswind direction respectively. The Bragg contribution of a facet is proportional to the 2-D wavenumber spectrum at the resonant wavenumber vector.

$$\sigma_0^{Br} \sim W(\vec{k}_B) \tag{34}$$

The contribution due to specular reflection is given by:

$$\sigma_0^{\mathrm{sp}} = \pi \mid R(0) \mid^2 \sec^4\theta P_S(\zeta_x, \zeta_y) \mid_{\mathrm{sp}} \tag{35}$$

Where P_S is the probability that a (specular) facet is oriented with tilts ζ_x (parallel) and ζ_y (right angles to radar look direction). For an anisotropic Gaussian surface one has:

$$P_S \mid_{\mathrm{sp}} = P_S(\zeta_x = \tan\theta, \zeta_y = 0) = \frac{1}{2\pi s_{u,s} s_{c,s}} \exp(-\frac{\tan^2\theta}{2s_{L,s}^2}) \tag{36}$$

In which $s_{u,s}^2$ and $s_{c,s}^2$ are the slope variances in the upwind and crosswind direction respectively, whereas $s_{L,s}^2$ is the variance in the radar look direction. Only those waves that have a wavelength longer than the radar wavelength contribute to the slope variances; shorter waves will not be seen by the radar (Stewart, 1985).

The above general two-scale theory has to be supplemented with a criterion to separate long waves from short ones. The 2-D wavenumber spectrum is separated into a low and high wavenumber part with the help of the splitting parameter k_c.

$$\begin{aligned} W_L(k,\alpha) = F_L(k)D(\alpha) \quad &= W(k,\alpha) \qquad k < k_c \\ &= 0 \qquad\qquad k \geq k_c \\ W_H(k,\alpha) = F_H(k)D(\alpha) \quad &= W(k,\alpha) \qquad k \geq k_c \\ &= 0 \qquad\qquad k < k_c \end{aligned} \tag{37}$$

Hence the slope variances of the tilting waves are given by:

$$s_{a,b}^2 = \frac{1+a_2}{2}\int_0^{k_c} k^3 F(k)dk \tag{38}$$

$$s_{c,b}^2 = \frac{1-a_2}{2}\int_0^{k_c} k^3 F(k)dk \tag{39}$$

Note that the slope variance of the waves that contribute to specular reflection is given by $s^2 = \int_0^{k_r} k^3 F(k)dk$.

The splitting parameter k_c is determined by the condition $\beta = 4k_0^2\sigma_H^2$, where $\sigma_H^2 = \int_{k_c}^{\infty} F(k)dk$. It can be argued that the parameter β should lie in the range 0.1-1 (Snoeij et al., 1992).

In the waves-scatter module the above integral expression for σ_0^{SEA} is numerically solved.

2.4 The inverse model

In order to use the VIERS model for wind retrieval from ERS-1 scatterometer data, it has to be inverted. The following simple but straightforward scheme has been used.

First a table of σ_0's is produced; the interpretative model is run for different incidence angles, wind vectors and wave periods and the resulting sigma's are collected in a table. The windparameters are U, the absolute value, and ϕ, the direction with respect to the lookdirection of the radar. In order to reduce the computational load the standard resolution used in VIERS was 1 m/s in wind speed and 15^o in wind direction. For this case the incidence angle runs from 18 until 57 in steps of 1, U runs from 1 until 30 in steps of 1 (m/s) and ϕ runs from 15 until 360 in steps of 15 (^{o}).

For tuning purposes the low resolution is sufficient; a higher resolution is, however, desirable when comparing different models. Therefore also a high resolution table has been produced with steps in wind speed of 0.5 m/s and wind direction of 5^o.

For a certain cell number i and measured sigma triplet $(\sigma_f, \sigma_m, \sigma_a)$ the wind retrieval procedure is as follows.

1. Determine incidence angles of for-, mid- and aftbeam: $\theta_f(i), \theta_m(i), \theta_a(i)$.

2. Calculate model triplets (for all 30×24 tabulated wind vectors $U = 1, 2..., 30$ and $\phi = 15, 30, ..., 360$) according to:

$$\begin{aligned} \sigma_f^{mod} &= \sigma^{tab}(\theta_f, U, \phi + 45) \\ \sigma_m^{mod} &= \sigma^{tab}(\theta_m, U, \phi) \\ \sigma_a^{mod} &= \sigma^{tab}(\theta_a, U, \phi - 45) \end{aligned} \tag{40}$$

Hence ϕ is the direction of the wind vector with respect to the midbeam.

3. Determine the normalized quadratic distance between model and measured triplets.

$$Q_{ERS-1} = Q_f + Q_m + Q_a$$

$$Q_{f,m,a} = (\frac{\sigma_{f,m,a} - \sigma^{mod}_{f,m,a}}{\kappa_p \sigma_{f,m,a}})^2$$

Here κ_p is the noise level (of the order of 5%); $\kappa_p \sigma$ is the measurement error in σ.

4. Determine the normalized quadratic distance between model and ECMWF wind (magnitude and direction).

$$Q_{EC} = (\frac{U - U_{EC}}{\Delta U_{EC}})^2 + (\frac{\phi + \chi_2 - \phi_{EC}}{\Delta \phi_{EC}})^2$$

Where χ_2 is the lookdirection of the midbeam with respect to north. The errors in the ECMWF wind fields are estimated as $\Delta U_{EC} = 2$ m/s and $\Delta \phi_{EC} = 20^o$.

5. Determine the absolute minimum of the cost function D.

$$D = \sqrt{Q_{ERS-1} + Q_{EC}}$$

6. The model wind that minimizes D is the 'retrieved wind'. The direction of the wind with respect to north, ϕ_W, is given by $\phi_W = \chi_2 + \phi_{\rm ret}$, where $\phi_{\rm ret}$ is the retrieved wind direction with respect to the midbeam.

The fourth step is inserted in order to ensure that the retrieved wind vector is close to the ECMWF one, both in magnitude and direction. This is a rather strong requirement that may introduce a spurious interdependence between retrieved and ECMWF winds. A better option might have been not to take Q_{EC} into account and remove the 180^o ambiguity in the retrieved wind by selecting the direction closest to ECMWF's.

2.5 Implementation

In the present report no details about the software will be given; the interested reader should consult the final VIERS-1 report (P. Janssen et al., 1995).

3 Model configuration

The scatterometer model as it is described in the previous section is the result of evolution. Originally the three submodels have been separately developed and tested. Once they had been fused together a number of problems occurred that asked for modifications. In this section we give an account.

The flexible part of the model is the stress-waves module. Most of its parameters and parametrizations are only poorly known; it is even unclear which are the relevant processes that govern the dynamics of the short waves (Jähne and Riemer, 1990). Hence, it was this module that was regularly modified to overcome various problems.

Of the other two modules the wind-stress module has never been changed, and the waves-scatter module only allows retuning of the numerical values of two parameters (β and $R(0)^2$), which were always adjusted *after* the modification of the stress-waves module.

3.1 Development of the stand-alone wave module

In the third phase of the VIERS project a proto-type stress-waves module, based on theoretical ideas, was used to generate wave spectra compatible with laboratory measurements. The module did not include the dissipation processes due to slicks and wave breaking, whereas the spectral joining point was at two to three times the peak frequency. Nevertheless the model was capable to produce realistic laboratory wave spectra over a considerable range of wind speeds. However, a number of shortcomings of this proto-type could be identified, a major problem was the determination of the numerical values of the coupling constants T_3 and T_4.

A test with a one-point WAM model revealed that the numerical value of the coupling constant T_4 should be 0.25. Furthermore it was found out that the coupling constant T_3 should be of the order unity in order to ensure that viscous damping plays a dominant role at low wind speeds. In the VIERS model a constant value of 3 for T_3 was found to work satisfactory; in SATVIEW a wind speed dependence was build in.

If one employs these values for the coupling constants, it turns out that too much energy is pumped into the spectral tail. This complication can be remedied by introducing additional dissipation processes like wave breaking and damping due to slicks. It is furthermore necessary to limit the energy flux due to nonlinear interactions from peak into tail; this can be done by putting f_{join} in the range 2-5 Hz. (For sea spectra the original f_{join} was too low, yielding an ε_0 that was too large.)

Linear and quadratic models for wave breaking have been investigated. It turned out that quadratic breaking was too strong at high winds: the spectrum was completely quenched and therefore this mechanism had to be discarded. Linear dissipation, on the other hand, did a better job: if $2 < \beta_1 < 2.4$ (WAM value for β_1 is 2.25) one gets spectra that are quite satisfactory.

In order to lower the spectral level at small wind speeds, slick damping was introduced. Parameters corresponding to a natural slick of biological origin were chosen and

this worked out fine for low winds. However, it was annoying that a residual damping effect remained even at high winds. However, slicks should be washed-down once the wind is strong enough (cf. Alpers and Hühnerfuss, 1989). This process has been modelled on an ad hoc basis by letting the dilatational modulus go to zero for strong winds: $E_s = 0.005(1 + \tanh(10u_* - 4.33))$.

A second modification in the slick modelling was necessary because it seems very unrealistic that the ocean is covered by a single large slick. Slicks come in patches and this can be modelled by a fractional filling factor F (Lombardini, 1986). For $F < 1$ the damping is modified according to $y_F(f) = 1/(1 - F + F/y_1(f))$, where y_1 is the damping when the coverage is complete. Typical F-values are in the range 0.88-0.99 (cf. Lombardini, 1986).

Along the lines sketched above (already anticipated in the third VIERS progress report, Snoeij et al., 1992) it was thus possible to contrive a model that complies with existing theoretical ideas and at the same time is able to generate realistic sea spectra. During this stage the exact numerical values of free parameters could not be determined. Only a rough tuning, in which the order of magnitude or domain range of parameters was inferred, was pursued.

3.2 Incorporation into the full model; interpretative mode

After the incorporation of the stress-waves module into the full scatterometer algorithm, the model output was critically looked at. The following procedure has been used.

First the σ_0's in the upwind direction ($\phi = 0$) were monitored as a function of incidence angle at different wind speeds. The sea state parameter (wave age or wave period) was not independent, but coupled to the wind speed (this is a good first approximation). The parameters and parametrizations in the stress-waves module were determined in such a way that the model curves at moderate windspeeds were as close as possible to the CMOD4 ones. (For a description of the CMOD4 model cf. Stoffelen and Anderson, 1995.) Subsequently the VIERS model was fed with ECMWF winds and WAM sea state data (hence in this case the sea-state parameter was not directely coupled to the wind). The wind and wave data were collocated with the ERS-1 scatterometer swath at a particular day (911106). The model σ_0's were compared to the σ_0's measured with the ERS-1 forbeam. The same comparison was made with model σ_0's obtained with the operational model CMOD4.

The first attempts revealed some incompatibilities between the model and the measurements: the small model σ_0's were 4 dB too high and the large model σ_0's were 4 dB too low. The first discrepancy could be remedied by the inclusion of a suitable slick, for the second one the model had to be extended. It turned out that the stress-waves module generated slope variances that were quite low. In fact they were too low (at low winds) to produce any significant specular reflection. It was concluded that the slope variance from the stress-waves module were no good and that they had to be augmented before putting them through to the waves-scatter module. Then it

was realized that the stress-waves module only calculates the wind-sea spectrum, thus neglecting swell. Therefore the slope variances were augmented by a fixed amount due to swell (of the order of 0.02, after fine-tuning the value 0.024 was fixed) before passed over to the waves-scatter module. In this manner damage to the consistensy of the model could be minimized.

The above procedure has been succesful in the sense that a good scatter plot for the VIERS model could be obtained, even better than the corresponding CMOD4 plot. The CMOD4 model generates very small σ_0's (much smaller than measured) at low wind speeds, whereas the VIERS model does not suffer from this problem. It turned out that this was a generic picture as the same features have been found at other dates and other beams.

3.3 Incorporation into the full model; inverse mode

It was expected that the inverted VIERS model fed with ERS-1 σ_0's and WAM wave data would yield wind fields compatible with collocated ECMWF fields. This turned out not to be the case: the model winds differed significantly from the ECMWF winds. Mean model winds were unequal to mean ECMWF winds.

The inversion procedure was not to blame for this as the same inversion applied to the CMOD4 model produced winds compatible with ECMWF. Apparently the tuning procedure in σ_0 space was not sound: the ECMWF winds produce too much scatter thus preventing a meaningful tuning.

A new tuning procedure was started aiming at compatible winds: the model winds should lie as close as possible (in a statistical sense) to the ECMWF winds. Not only should the model winds follow ECMWF in the mean, but also should the variance be minimal. Special care was given to winds higher than 15 m/s; it is suggested that ECMWF wind speeds in this regime are 15% too low. Therefore the very high winds were not tuned at ECMWF values, but at the anticipated higher values. In a later stage another requirement was added: the statistics of the cost function should be optimal (i.e. average costs as low as possible). This latter condition ensures that the interrelation between the three beams is reproduced as good as possible; it is a measure of how good the cone-shaped figure in $\vec{\sigma}_0$ space is represented.

Hence, the major problem to be overcome was that in the regime of high wind speeds the VIERS winds were too low. It turned out that this problem was connected to the parametrization of the Phillips constant α_P. Therefore the original JONSWAP parametrization, $\alpha_P = 0.52\xi^{-1.41}$, was dropped and replaced by $\alpha_P = A\xi^{-B}$ (A and B to be determined). After a cumbersome tuning exercise the values $A = 0.24$ and $B = 1$ were selected for the VIERS model. In SATVIEW a retuning for A and B appeared necessary.

After the problems with the high winds had been eliminated, the low wind speed regime was tackled. Critical processes here are wave breaking and slick dissipation. By giving these processes appropriate weights optimal wind fields could be retrieved.

A weak point of the VIERS model is that its performance depends critically on

the precise parametrization of f_{join} and a_2 (as a function of u_*), whereas there are no theoretical guidelines what they should be. As far as a_2 is concerned, the CMOD4 model gives some empirical hints, which have been followed.

3.4 Fine-tuning of the model

Several parameters in the wave module are not fixed a priori, the most important being f_{join}, a_2 and α_P. The model output depends critically on the precise choice of f_{join} and a_2 as a function of u_* and of α_P as a function of the wave age. These three variables were the basic tuning parameters.

For the final fine-tuning the following procedure was adopted. About 30.000 σ_0 triplets, measured with the ERS-1 scatterometer at 6^{th} November 1991, together with collocated WAM information on the spectral peak (period of the dominant waves) were fed into the inverted VIERS model. The produced model winds (magnitude and direction) were plotted against collocated winds calculated by the numerical wether prediction model at ECMWF. The tuning parameters f_{join}, a_2 and α_P were chosen in such a way that the average bias and variance (between VIERS and ECMWF winds) were as low as possible and the spectra of the wave module of the best quality. This method ensures that the VIERS and ECMWF winds are compatible in a statistical sense. The results of the tuning exercise can be found in the final VIERS-1 report (P. Janssen et al., 1995).

4 Model validation

The VIERS modelwinds have been validated in a statistical sense against ECMWF data at two other dates; in addition a qualitative comparison with synoptic windfields in the Norwegian Sea showed good model performance (P. Janssen et al., 1995).

However, a major defect in $\vec{\sigma}$-space has been detected (P. Janssen et al., 1995). It turns out that if VIERS modelwinds are used to generate (in the interpretative scatterometeralgorithm) σ_0's, the latter deviate from measured σ_0's. This misfit has been tackled in the SATVIEW project.

4.1 A measure for model imperfection

The error statistics of the radar backscatter measurement are such that the three beams are considered to be independent and that the absolute (i.e. not in dB) σ_0 is a Gaussian variable with a 5% standard deviation. It is assumed that the error statistics of the ECMWF variables U_{EC} and ϕ_{EC} also follow the Gaussian law (standard deviation 2 m/s respectively 20^o).

Given the error statistics, the distribution of the minimum of the cost function, $D_{\min}$, can be calculated for a perfect model. In practice an actual model may not be perfect. This manifests itself in a shift of the distribution of $D_{\min}$ towards higher costs. The smaller the shift, the better the model.

This qualitative idea can be put into a quantitative measure as follows. Assume that the statistics of the minimal cost $D_{\min}$ is determined by n independent Gaussian variables δ_i.

$$D^2_{\min} = \sum_{i=1}^{n} \delta_i^2 = \sum_{i=1}^{n} Q_i \tag{41}$$

δ_i is the normalized deviation due to measurement errors between model variable i and actual measurement, $< \delta_i >= 0, < \delta_i^2 >= 1$.

An elementary result in statistics states that the distribution of $D^2_{\min}$ is chi-square with n degrees of freedom. This result is valid if the assumption of Gaussian variables is justified and if the model at hand is perfect.

Nevertheless in practice the actual distribution may deviated from the theoretical one. The discrepancy is due to random model errors (it is assumed that all systematic errors are eliminated) that widen the distribution of δ_i; e.g. the inversion procedure may introduce errors. In stead of unit variance one will have $< \delta_i^2 >= 1 + f_i^2$, where f_i^2 is the additional variance due to fluctuating model errors (these are assumed to be Gaussian and statistically independent from the measurement errors). The model error in the i$^{\text{th}}$ model variable may now be defined as f_i times the measurement error in the i$^{\text{th}}$ variable.

4.2 Model comparison

Both VIERS and CMOD4 have been well-tuned to the ECMWF winds. But how well do both scatterometer models reproduce σ_0 triplets? The histograms for the minimal cost $D_{\min}$ give the answer.

As one can see in figure 2 the CMOD4 model has systematically lower overall costs than the VIERS model. As both models reproduce the ECMWF windfield equally well, this means that the CMOD4 model reproduces the σ_0 triplet better than does the VIERS model.

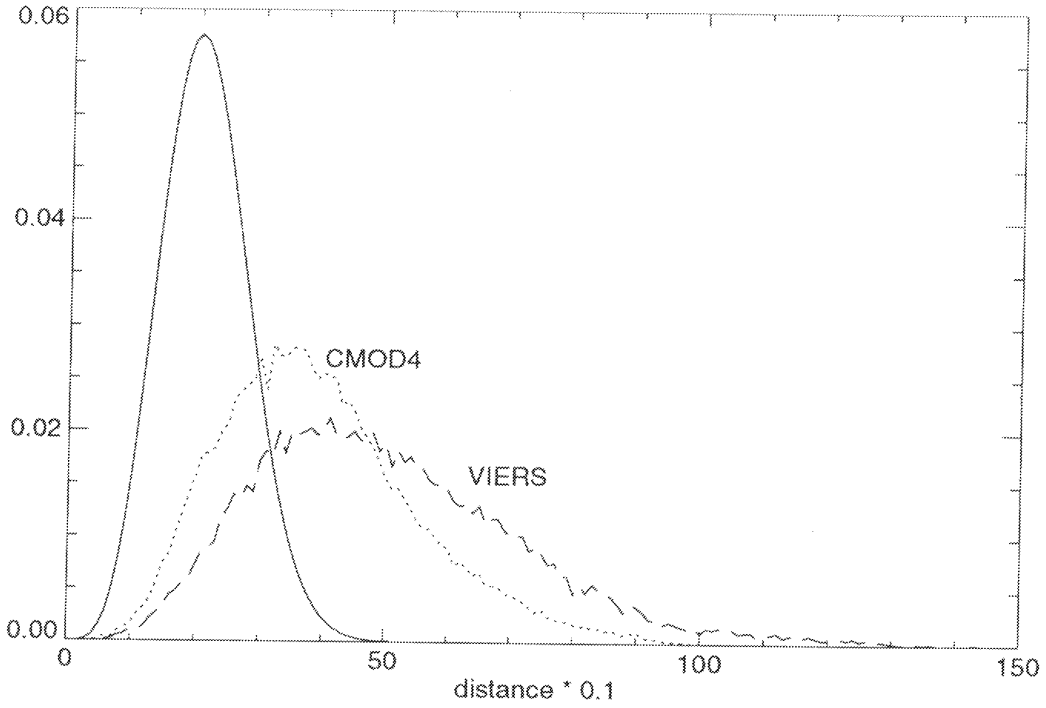

Figure 2: Normalised histograms of minimal costs for VIERS and CMOD4 (low resolution).

It can also be seen in figure 2 that there is a significant gap with the perfect model. However, this gap is primarily due to the low resolution of the inversion table as described in section 2.4. At higher resolution the gap diminishes.

The quantitative analysis of the individual costs has been summarized into tables 1 and 2. From these tables it can be concluded that both models model the ECMWF winds far better than the ERS-1 σ_0's. Clearly the CMOD4 model gives a better reproduction of the σ_0 triplet than does VIERS. In quantitative terms one can say that the model error in reproducing σ_0 is about 6.5% for CMOD4 and about 13% for VIERS.

model	$< Q_1 >$	$< Q_2 >$	$< Q_3 >$	$< Q_4 >$	$< Q_5 >$	total
perfect	1.00	1.00	1.00	1.00	1.00	5.0
CMOD4	2.47	3.22	2.35	1.02	2.01	11.1
VIERS	7.65	7.85	7.15	1.03	1.98	25.7
SATVIEW	2.39	3.69	2.13	1.27	1.87	11.4

Table 1: Mean minimal costs at 911106 (N=29752, high resolution).

model	$< Q_1 >$	$< Q_2 >$	$< Q_3 >$	$< Q_4 >$	$< Q_5 >$	total
perfect	1.00	1.00	1.00	1.00	1.00	5.0
CMOD4	2.22	3.10	2.29	1.46	1.46	10.5
VIERS	7.30	8.78	7.90	1.37	1.47	26.8
SATVIEW	1.99	3.29	2.06	1.72	1.36	10.4

Table 2: Mean minimal costs at 920310 (N=30049, high resolution).

Note that we have also included the results of the SATVIEW model in table 1 and 2; the discussion of these results will however be postponed till the next section. A final note concerns the relative high values of $< Q_1 >$, $< Q_2 >$ and $< Q_3 >$ with respect to $< Q_4 >$ and $< Q_5 >$. This is caused by the inversion procedure that assimilates ECMWF wind-field data. If these data are discarded and a cost function that only contains Q_1, Q_2 and Q_3 is used, the values of $< Q_1 >$, $< Q_2 >$ and $< Q_3 >$ may drop. This matter will, however, not be further investigated here.

5 The SATVIEW approach

It is well-known that measured triplets of normalized radar cross-sections at fixed cell number approximately fall on a two-dimensional cone-shaped manifold in $\vec{\sigma}$-space. A triplet may be denoted by $(\sigma_1, \sigma_2, \sigma_3)$, where the σ's respectively refer to for-, aft- and mid-beam. A cross-section through the plane $\sigma_1 + \sigma_3 =$ constant produces a ring- or egg-shaped scatter plot with axes spanned by $\sigma_1 - \sigma_3$ and σ_2.

An adventious and simplifying circumstance is that the eggs may be turned into circles if a logarithmic scale is introduced, i.e. in the variables $x = (\sigma_1 - \sigma_3)/(\sigma_1 + \sigma_3)$ and $y = \ln(\sigma_2/(\sigma_1 + \sigma_3))$ an almost circular scatter plot is obtained.

A scatterometer algorithm should be calibrated such that its model manifold coincides with the center of gravity of a large number of measured triplets. For the VIERS algorithm this condition is not completely fulfilled: the model circles are in some cases smaller than the measured ones. Nevertheless, the VIERS algorithm produced wind fields with realistic frontal structures (P. Janssen et al., 1995).

This paradoxical state of affairs can be understood if one considers the usual wind retrieval procedure. A measured triplet is projected onto the model manifold to obtain its model counterpart. In the xy-plane in $\vec{\sigma}$-space this amounts to projection on a circle. The direction of projection corresponds to the retrieved wind direction, and it is obvious that this direction is independent of the size of the circle. Hence a mismodelled circle doesn't deteriorate the retrieved wind direction.

The simplest scatterometer algorithm, which neglects the upwind-downwind asymmetry, is of the following form.

$$\sigma = b_0(1 + b_2 \cos(2\phi)) \tag{42}$$

The coefficients b_0 and b_2 depend on wind speed and cell number (or incidence angle), whereas ϕ is the azimuthal angle between radar lookdirection and windvector.

In terms of this model function the above paradox can be rephrased as follows: *for wind retrieval* the parametrization of b_2 is not very critical. However, this message should not be considered as a permit not to go for the best b_2-parametrization.

The above equation provides an approximate description of the directional properties of radar backscattering. Through the Bragg mechanism the radar directionality is related to the directional distibution of the resonant water waves, the spectral function $D(\alpha)$ of which may be described by

$$D(\alpha) = \frac{1}{2\pi}(1 + 2a_2 \cos(2\alpha)) \tag{43}$$

In case of pure Bragg scattering one would have $2a_2 = b_2$.

On physical and practical grounds the anisotropy coefficient a_2 in the VIERS model has been allowed to only depend on wind speed, such that increased wind speed implies increased anisotropy. The background for this simplifying description was that there is no obvious manageable physical process that would cause the directional properties of waves of different wavelength to be different (the full non-linear interaction source

term requires a non-economical amount of computer power). However, an additional dependence of a_2 on resonant wavelength (or equivalently on cell number or incidence angle) is clearly needed in order to reproduce the full cone-structure in $\vec{\sigma}$-space.

The usual and appropriate way to monitor the goodness-of-fit of measured and modelled triplets is by means of a cost function: a misfit manifests itself in high costs. The SATVIEW approach to eliminate the relative high costs of VIERS cycle 2.0 consists of several steps. First ERS-1 scatterometer data together with collocated ECMWF wind field data have been used to obtain the coefficient b_2 at different wind speeds and incidence angles (cell numbers). Taking successive slices of 100 points at nearly constant $\sigma_1 + \sigma_3$ (hence at nearly constant wind speed) in the xy-plane (see above), we have determined b_2 as the circular radius having minimal costs. The discrete set of b_2-values thus obtained is then, with the use of an appropriate function, parametrized in terms of wind speed and radar incidence angle. This route yields an objective b_2, which is to be preferred to the subjective approach followed in (Stoffelen and Anderson, 1995). Subsequently, the optimal b_2-parametrization is equalled to two times the directional anisotropy coefficient a_2, and build in into the VIERS model. Finally, a retuning exercise is needed to ensure that the VIERS model produces realistic wave spectra and wind fields.

The following a_2-parametrization has been obtained.

$$a_2 = cU_{10}^{\alpha} \exp(-\beta U_{10}^{\gamma}) \tag{44}$$

with $c = 0.0525$, $\alpha = 1$, $\beta = 6.5\exp(-5.7\theta)$ and $\gamma = 0.235\theta^2 + 1.486\theta - 0.273$. The incidence angle θ is in radians. A graphical representation of this parametrization has been depicted in figure 3; the lower curve is at $\theta = 25^o$, subsequently θ increases with 5^o.

It can be clearly seen that there is a considerable wind dependence of a_2. Resonant waves corresponding to high incidence angles get progressively directed at increasing wind speeds up to 10-12 m/s; at higher wind speeds wave spreading is enhanced and a_2 diminishes.

The above a_2 replaces the original VIERS parametrization ($a_2 = 0.097 + 0.095u_* + 0.059\tanh(20u_* - 2.93)$). Due to the high complexity and parameter sensitivity such an operation requires an extensive retuning of the model parametrizations to ensure that wave spectra, retrieved winds and costs satisfy all physical and practical conditions. An iterative procedure was followed in which the key parameters f_{join}, T_3 and α_P were first selected to produce well-structured wave spectra. Subsequently a statistical analysis of retrieved winds and histograms of minimal costs (cf. section 4.2) was performed. The emerging picture in combination with the known interdependence of the various parameters yielded the direction to further optimize the tuning parameters, in particular f_{join}, T_3 and α_P.

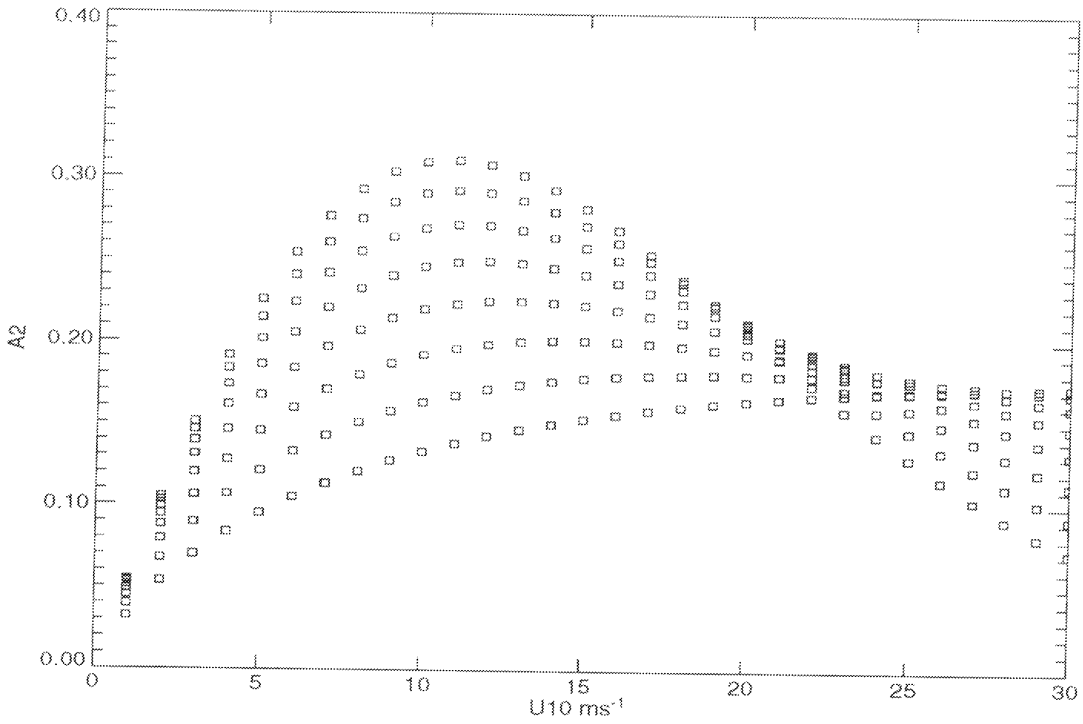

Figure 3: SATVIEW α_2-parametrization. (θ=25,30,35,40,45,50,55,60)

After going through this cycle several times the following parametrizations were obtained.

$$f_{\text{join}} = 35.7 u_*^{0.28} \exp(-2.305 u_*^{0.25}) \tag{45}$$

$$T_3 = 6.58 + 3.55 \tanh(10 u_* - 4) \tag{46}$$

$$\alpha_P = 0.13 \xi^{-0.78} \tag{47}$$

The improvement in terms of total costs of the SATVIEW parametrizations compared to the original VIERS parametrizations, has been graphically demonstrated in figures 4 and 5, where the model costs of approximately 30.000 datapoints collected at November 6^{th} 1991, which appears to be a statistically representative sample, have been plotted as normalized histograms. In figure 4 the misfit of VIERS is clearly visible, whereas figure 5 suggests that the SATVIEW fit is as good as the CMOD4 parametrization.

A quantitative summary of the individual costs of the relevant models can be found in the tables 1 and 2. These data clearly demonstrate the good representation in backscatter space of the SATVIEW model; SATVIEW performs comparably with CMOD4.

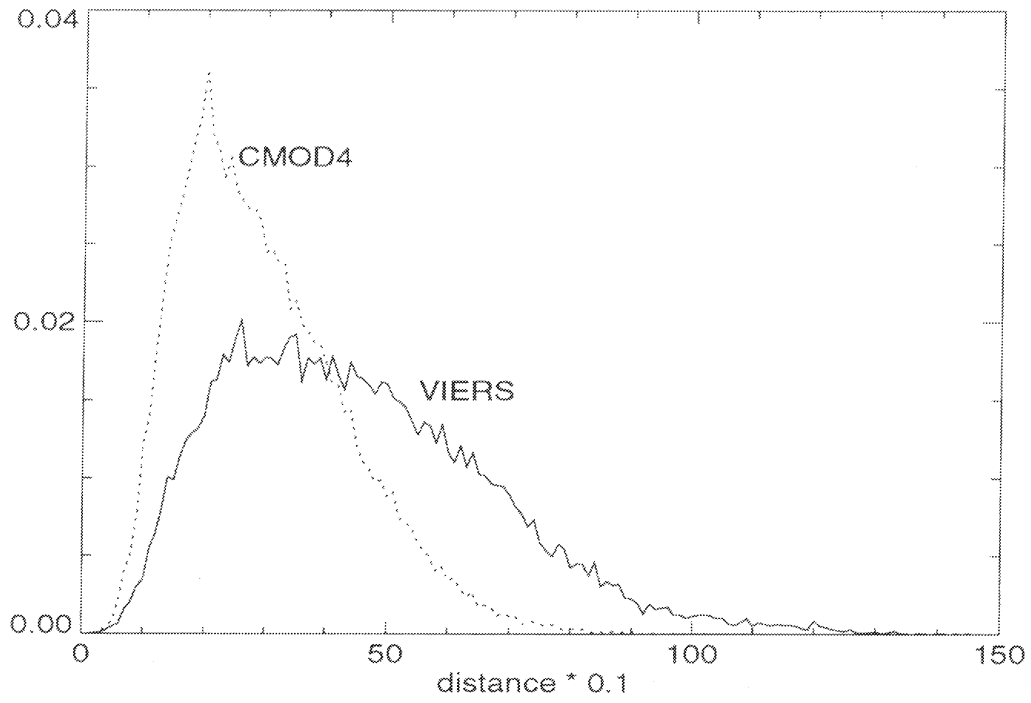

Figure 4: Histograms of VIERS and CMOD4 costs (high resolution).

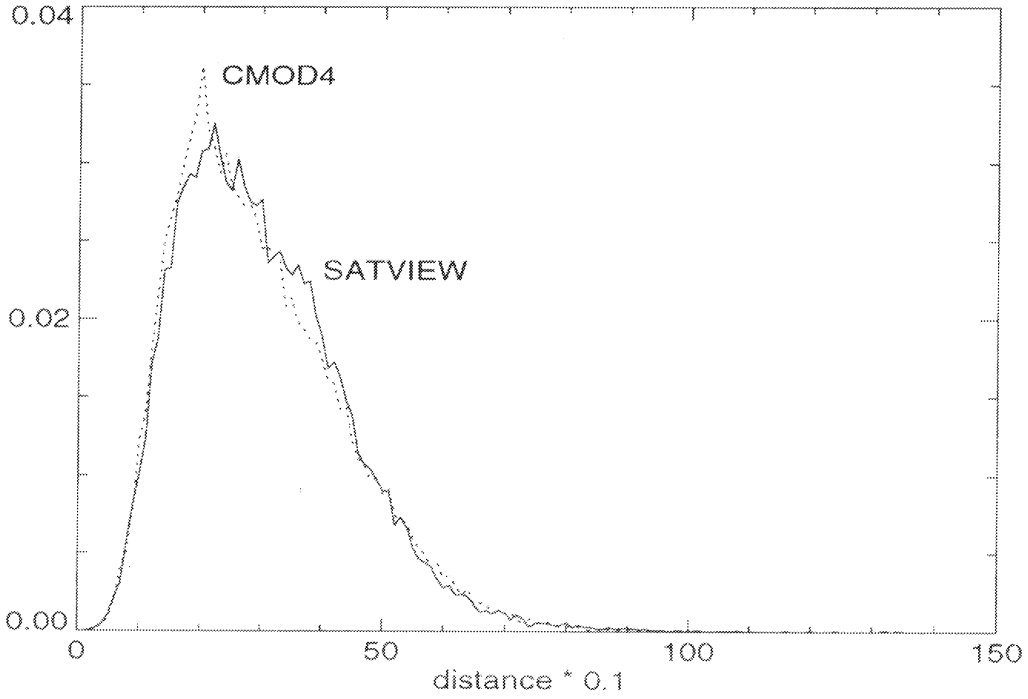

Figure 5: Histograms of SATVIEW and CMOD4 costs (high resolution).

In the figures 6, 7 and 8 the statistics of retrieved wind speeds have been presented. In order to visualize the density of points in these plots, contour lines of equal density (number of points per square m/s) have been drawn. The algorithms of CMOD4, VIERS cycle 2.0 and SATVIEW all produce, in the statistical sense, wind speeds that are compatible with collocated ECMWF ones and have about the same amount of scatter. The same picture emerges for the wind direction. In the figures 9, 10 and 11 we have plotted retrieved wind directions versus ECMWF wind directions for the CMOD4, VIERS cycle 2.0 and SATVIEW algorithms respectively.

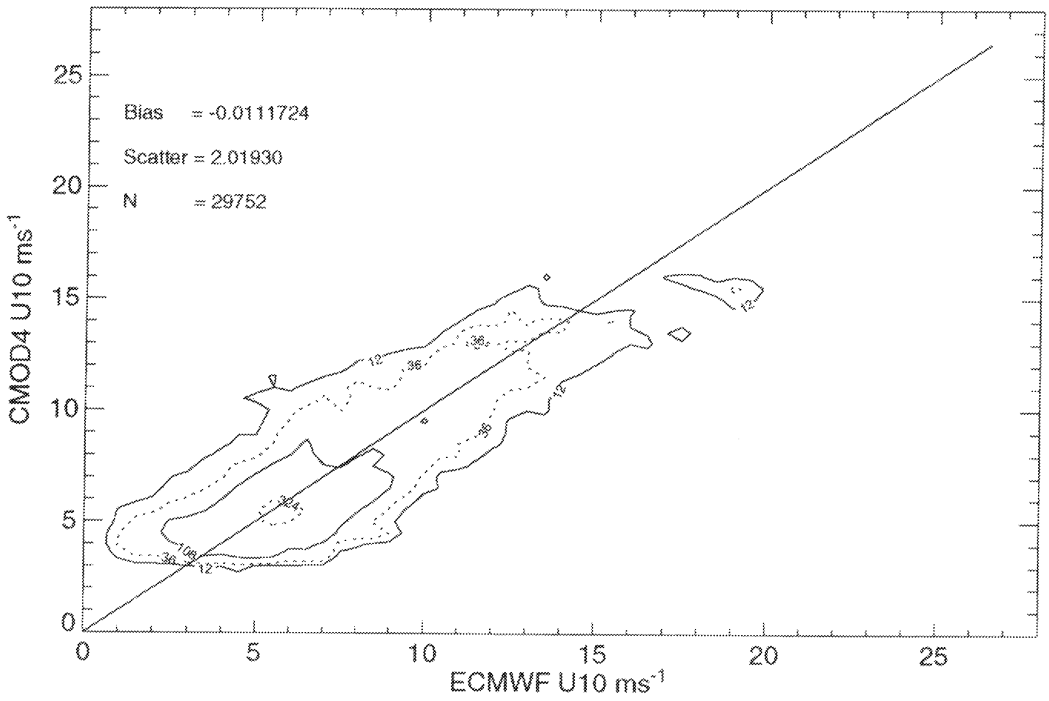

Figure 6: Scatterplot of CMOD4 retrieved winds vs. ECMWF winds (high resolution).

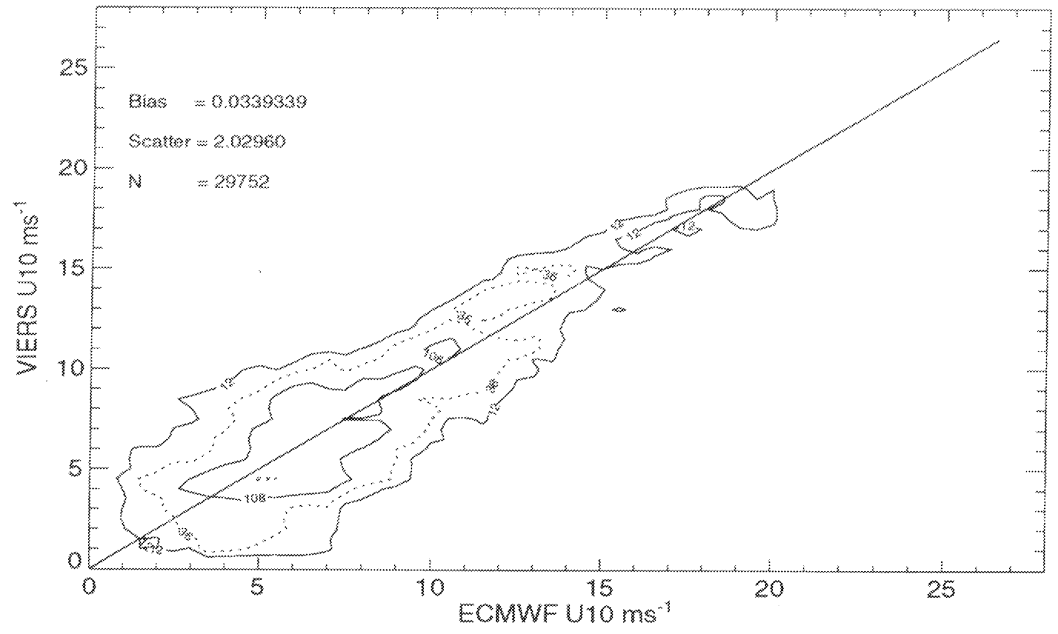

Figure 7: Scatterplot of VIERS retrieved winds vs. ECMWF winds (high resolution).

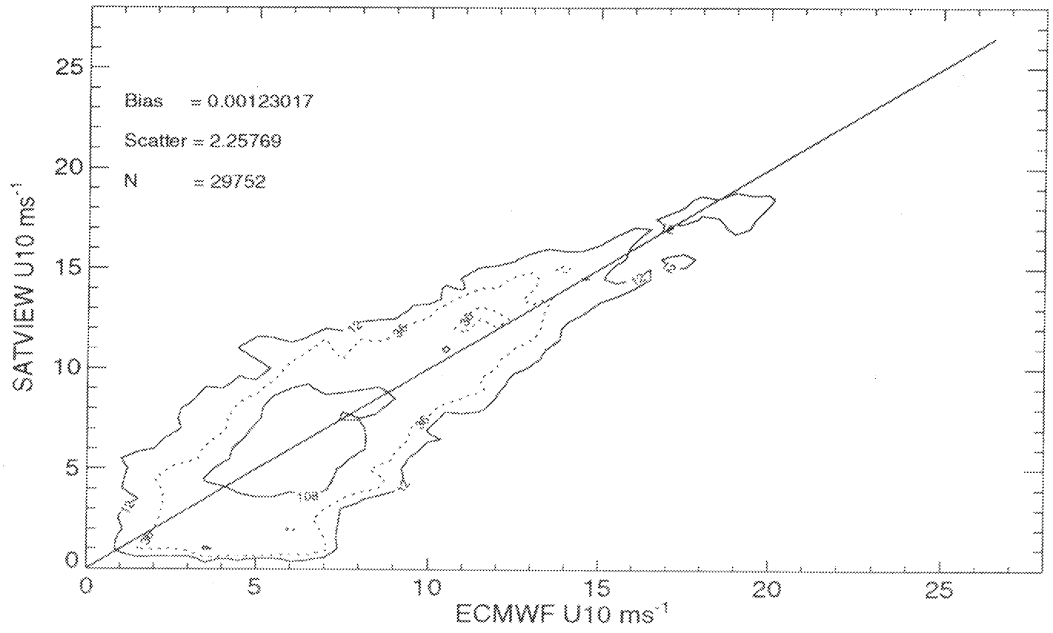

Figure 8: Scatterplot of SATVIEW retrieved winds vs. ECMWF winds (high resolution).

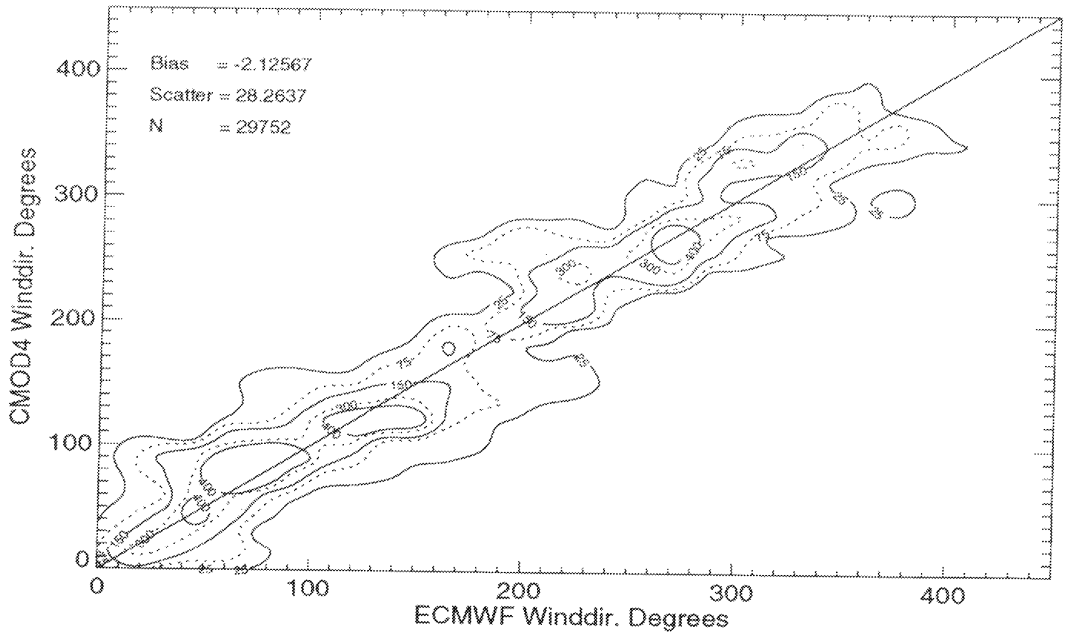

Figure 9: Scatterplot of CMOD4 retrieved wind directions vs. ECMWF wind directions (high resolution).

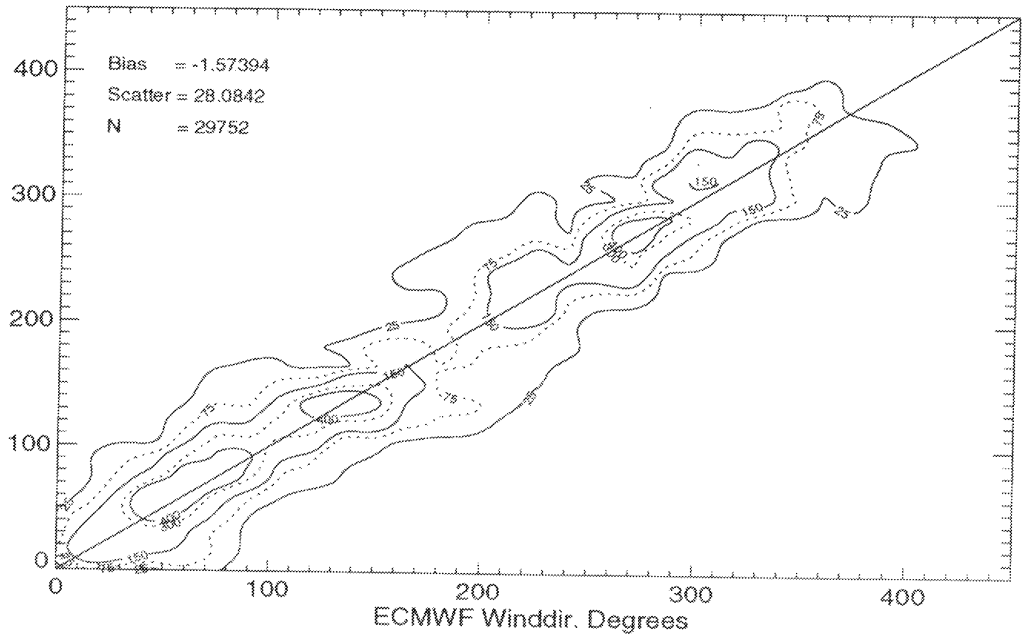

Figure 10: Scatterplot of VIERS retrieved wind directions vs. ECMWF wind directions (high resolution).

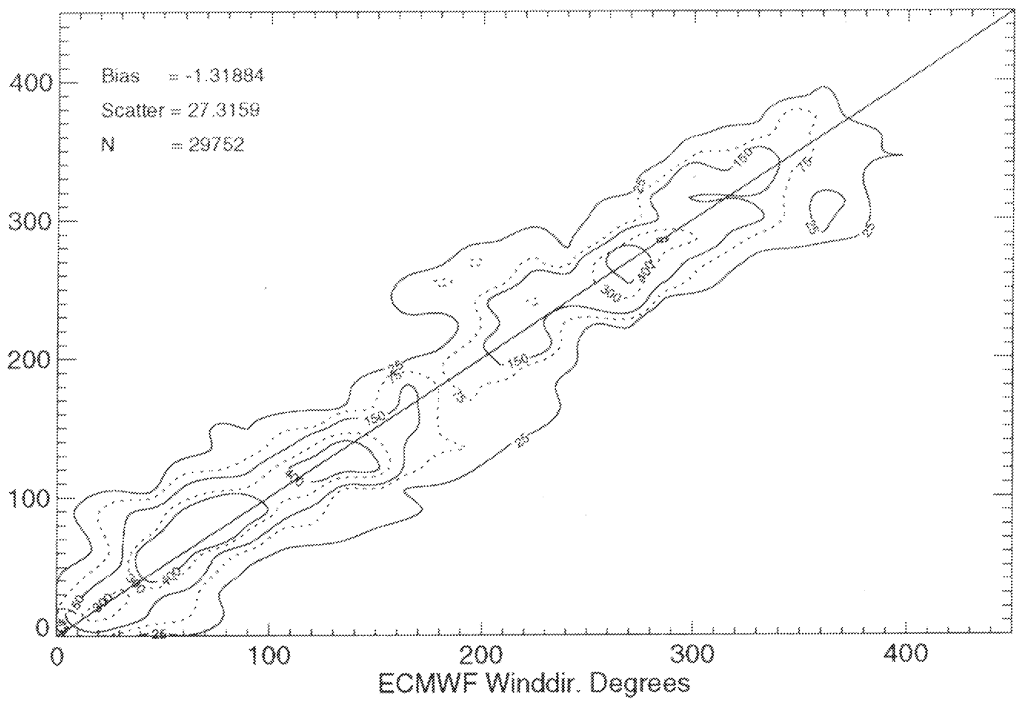

Figure 11: Scatterplot of SATVIEW retrieved wind directions vs. ECMWF wind directions (high resolution).

Finally, we picture the SATVIEW model wave spectra for the wind speed range 1 - 30 m/s. In figure 12 the 1-D frequency spectra have been depicted. It can be seen that the peak frequency shifts towards lower frequencies at increasing wind speeds, and that the spectral tail level rises as the wind speed increases. Another realistic feature is the quenching of the tail at low wind speeds (1 - 5 m/s). In figure 13 the tail structure has been magnified by plotting the spectral saturation parameter $B_{\rm sat}$, where $B_{\rm sat} = (2\pi)^4 f^5 E(f)/(2g^2)$. In comparison with the VIERS spectra the SATVIEW spectra are of a better quality. On the one hand this is due to a better tuning, but on the other hand the calculation of the spectra is done on a finer grid (300 grid points instead of only 100).

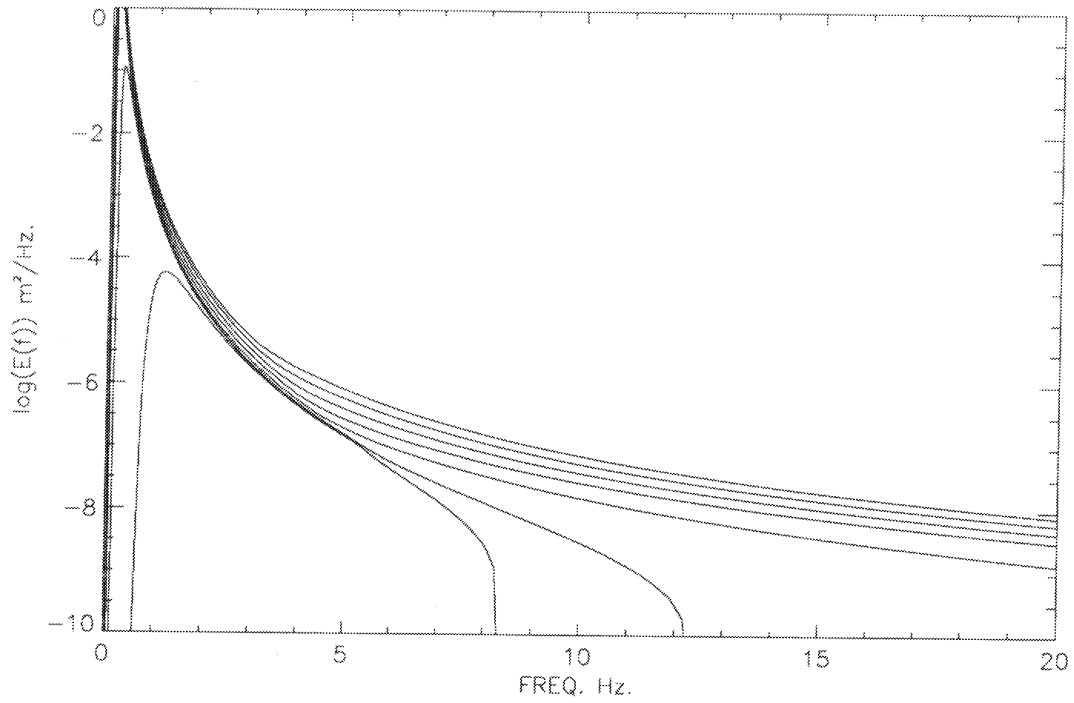

Figure 12: SATVIEW 1-D frequency spectra at $U10$=1,5,10,15,20,25,30.

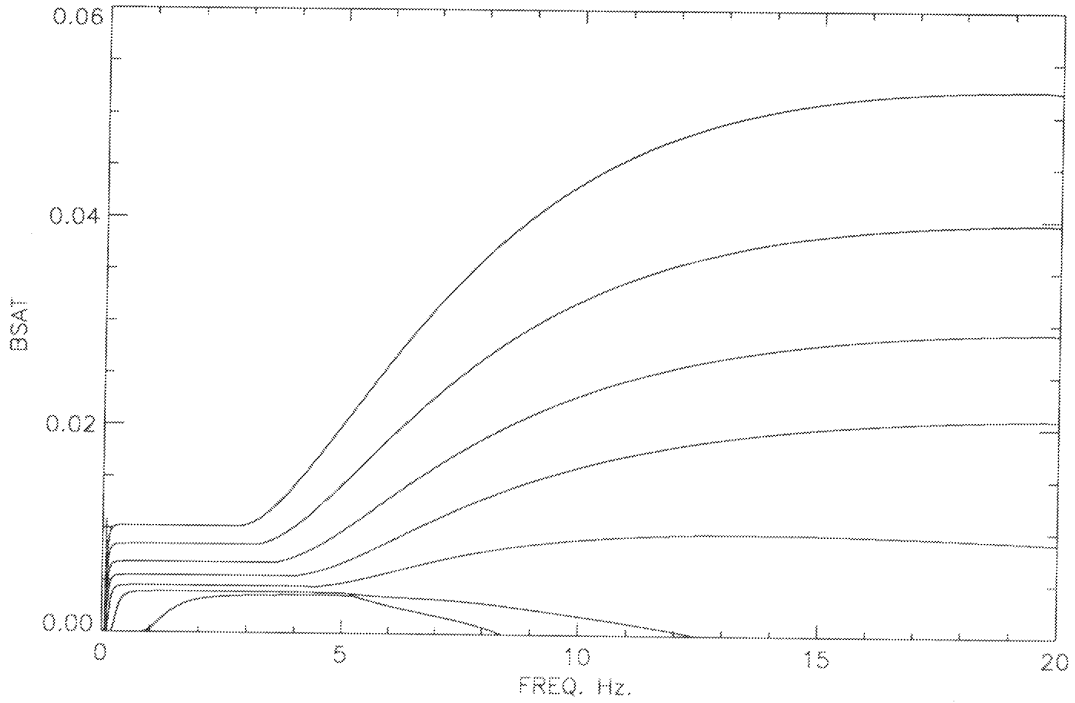

Figure 13: SATVIEW spectral saturation levels at $U10$=1,5,10,15,20,25,30.

6 Conclusion

The physics of scatterometry includes a number of processes: electro-magnetic interaction of radar beam and water surface, turbulence in the atmospheric boundary-layer, the formation of water waves due to wind, their destruction due to breaking and viscosity, the angular dispersion of water waves and other transformations due to non-linear interactions. Not all of these processes are equally well understood. Concerning the backscatter process, it has been generally accepted that a two-scale Bragg description is a good approximation and this has been confirmed by the VIERS project.

The interaction between atmosphere and ocean, and in particular the dynamics of water waves, pose more theoretical problems. In VIERS a framework based on a four-term energy balance equation for the 1-D elevation spectrum of resonant water waves has been adopted, which seems to work. However, it is not clear why it works: because it is fundamentally sound, or because the delicate tuning of unfixed parameters made it work.

The process of angular wave spreading had only been very roughly parametrized in the VIERS model, resulting in misfits in $\vec{\sigma}$-space. In the SATVIEW project the directional properties of the ERS-1 scatterometer have been thoroughly investigated. On the basis of this empirical information we have manufactured a better parametrization for angular wave dispersion. It should be borne in mind, however, that the physics of this process has not been explained, only an empirical parametrization has been obtained. Hence, the SATVIEW algorithm is a semi-theoretical, semi-empirical model.

From a practical point of view (wind retrieval) the performance of the SATVIEW algorithm appears to be fully satisfactory: its statistics are comparable with the operational CMOD4 model. What remains to be done, however, is to further investigate the physics of gravity-capillary waves, and in particular the process of angular wave spreading. Once there is more insight into these matters, one can go for a full physical scatterometer algorithm.

7 Acknowledgements

The authors wish to thank Dr. W.A. Oost and Dr. G.J. Komen for supporting this project. We are furthermore indebted to the VIERS group who handed over the VIERS and CMOD4 models.

8 References

Alpers, W. and Hühnerfuss, H.: 1989, 'The Damping of Ocean Waves by Surface Films: A New Look at an Old Problem'. *J. Geophys. Res.* **94**, 6251-6265.

Barthel, K., and Breivik, O.,: 1996, 'A physical scatterometer model function with input from a wave model', Report University of Bergen, Norway.

Businger, J.A., Wyngaard, J.C., Izumi, I., and Bradley, E.F.: 1971, 'Flux-profile relationships in the atmospheric surface layer'. *J. Atmosph. Science* **28**, 181-189.

Calkoen, C.J., Van Halsema, D., Jähne, B., Janssen, J.A.M., Oost, W.A., Snoeij, P., and Vogelzang, J.: 1990, 'VIERS-1 progress report part-2'. BCRS technical report No 90-27, 140 pp.

Cavanie, A. and Lecomte P.: 1987, 'Final report of ESA contract No 6874/87/CP-I(sc)', ESA publications division, ESTEC.

Donelan, M. A. and Pierson, W. J.: 1987, 'Radar Scattering and Equilibrium Ranges in Wind-Generated Waves with Application to Scatterometry', *J. Geophys. Res.* **92**, 4971-5029.

Dyer, A.J., and Hicks, B.B.: 1970, 'Flux-gradient relationships in the constant flux layer'. *Q. J. Royal Meteorol. Soc.* **96**, 715-721.

Hasselmann, K., Barnett, T.P., Bouws, E., Carlson, H., Cartwright, D.E., Enke, K., Ewing, J.A., Gienapp, H., Hasselmann, D.E., Kruseman, P., Meerburg, A., Müller, P., Olbers, D.J., Richter, K., Sell, W., and Walden, H.: 1973, 'Measurements of wind-wave growth and swell decay during the Joint North Sea Wave Project (JONSWAP)', *Dtsch. Hydrogr. Z. Suppl.* **A8(12)**, 95 pp.

Jähne, B. and Riemer, K.: 1990, 'Two-Dimensional Wave Number Spectra of Small-Scale Water Surface Waves'. *J. Geophys. Res. Oceans* **95**, 11531-11546.

Janssen, J.A.M., Calkoen, C.J., Van Halsema, D., Jähne, B., Janssen, P.A.E.M., Oost, W.A., Snoeij, P., Vogelzang, J., and Wallbrink, H: 1993, 'The VIERS scatterometer algorithm', in International Air-Sea Interface Symposium, Marseille, 1993.

Janssen, J.A.M.: 1996, 'Does wind stress depend on sea-state or not? - A statistical error analysis of HEXMAX data'. Accepted by Boundary-Layer Meteorol.

Janssen, P.A.E.M., Lionello, P., and Zambresky, L.: 1989, 'On the interaction of wind and waves', *Phyl. Trans. R. Soc. London*, **A329**, 289-301.

Janssen, P.A.E.M., Wallbrink, H., Calkoen, Ch., Van Halsema, E., Janssen, H., Oost, W., and Snoeij, P.: 1994, 'VIERS-1 FINAL Report Phase 4A'. BCRS contract report No 93-25, 9 pp.

Janssen, P.A.E.M., Calkoen, C.J., Van Halsema, D., Oost, W.A., Snoeij, P., and Wallbrink, H.: 1995, 'VIERS-1 Final Report Phase 4'. BCRS technical report No 95-14, 79 pp.

Komen, G. J., Hasselmann, S., and Hasselmann, K.: 1984, 'On the existence of a fully developed wind-sea spectrum'. *J. Phys. Oceanogr.* **14**, 1271-1285.

Lamb, H.: 1932, 'Hydrodynamics', 6th ed., Dover, New York, 738 pp.

Lombardini, P.P.: 1986, 'Maximum of damping ratio in rippled water covered by monomolecular films'. ONRL Report on the Role of Surfactant Films on the Interface Properties of the Sea Surface F.L. Herr and J. Williams, Ed. Office of Naval Research, London, Rep. **C-11-86**, 157-173.

Phillips, O.M.: 1958, 'The equilibrium range in the spectrum of wind-generated waves', J. Fluid Mech. **4**, 426-434.

Pierson, W.J. and Moskowitz, L.: 1964, 'A proposed spectral form for fully developped wind sea based on the similarity theory of S. A. Kitaigorodskii',*J. Geophys. Res.* **69**, 5181-5190.

Plant, W.J.: 1980, 'On the steady-state energy balance of short gravity wave systems'. *J. Phys. Oceanogr.* **10**, 1340-1352.

Plant, W.J.: 1990, 'Surface waves and fluxes', Eds. Geernaert, G.L., and Plant, W.L., 2 vols., Kluwer, Dordrecht.

Smith, S.D., Anderson, R.J., Oost, W.A., Maat, N., DeCosmo, J., Katsaros, K.B., Davidson, K.L., Bumke, K., Hasse, L., and Chadwick, H.M.: 1992, 'Sea surface wind stress and drag coefficients: the HEXOS results', *Boundary-Layer Meteorol.* **60**, 109-142.

Snoeij, P., Van Halsema, E., Vogelzang, J., Waas, S., Zecchetto, S., Janssen, H., Oost, W., Jähne, B., and Calkoen, Ch.: 1992, 'VIERS-1 Final Report Phase 3'. BCRS technical report No 92-24, 164 pp.

Stewart, R.H.: 1985, 'Methods of Satellite Oceanography', University of California Press, 360 pp.

Stoffelen, A. and Anderson D.: 1995, 'The ECMWF Contribution to the Characterisation, Interpretation, Calibration and Validation of ERS-1 Scatterometer Backscatter Measurements and Winds, and their use in Numerical Weather Prediction Models'. ECMWF technical report under ESA contract number 9097/90/NL/BI, 92 pp.

Valenzuela, G. R.: 1978, 'Theories for the interaction of electromagnetic and oceanic waves - a review'. *Boundary-Layer Meteorol.* **13**, 612-685.

Van Halsema D., Calkoen, Ch., Jaehne, B., Oost, W.A., Snoeij, P., and Waas, S.: 1989, 'Progress report on the VIERS-1 project part-1: the Delft wind/wave experiment'. BCRS technical report No 89-24, 128 pp.